Parametric motion of energy levels in quantum chaotic systems. I. Curvature distributions

Jakub Zakrzewski* and Dominique Delande
Laboratoire de Spectroscopie Hertzienne de l'Ecole Normale Supérieure, Université Pierre et Marie Curie, T12-E1, 4 place Jussieu, 75272 Paris CEDEX 05, France
(Received 6 October 1992)

The motion of energy levels in quantum systems that show a chaotic classical limit is statistically analyzed. A *quantitative* comparison is made between the tails of the curvature distribution and numerical results obtained for various physical models. Approximate analytic expressions for the full curvature distribution are derived from the statistical mechanics of a fictitious gas in a refined formulation that recovers the random-matrix theory for an arbitrary number of levels. They provide a better description of numerical data than just the tail-limiting expressions available previously. Good agreement with numerical data for various physical systems as well as for a model random dynamics is obtained with the *ad hoc* introduced very simple analytic expressions containing no free parameter. The nonuniversal behavior of small curvatures is discussed. The data obtained for the magnetized hydrogen atom support the previous interpretation of this phenomenon as due to the "scarred" wave functions. A large number of analyzed data allows us to show that the details of the curvature distribution provide a qualitative measure of the degree of scarring in different systems.

PACS number(s): 05.40.+j, 05.45+b

I. INTRODUCTION

Although developed about thirty years ago in an attempt to characterize complicated spectra of compound nuclei, random-matrix theory (RMT) [1, 2] found its recent successful application in describing properties of quantum spectra of simple systems which show classically chaotic behavior [3–5]. Low-dimensional systems, in contrast to nuclear physics problems where the exact form of the Hamiltonian is unknown, offer a unique opportunity for studying the connection between RMT and the deterministic dynamics, as generated by a typically nonrandom and strongly correlated Hamiltonian matrix. The connection between RMT and quantally chaotic dynamics is not yet fully understood, although some progress in this direction has been obtained in statistical-mechanics formalism (see [4] for a good systematic account of such attempts).

Until very recently, "quantum chaos" applications of RMT were limited to the comparison of its predictions with the statistical properties of energy eigenvalues and eigenvectors for well-defined model or realistic *single* systems. The knowledge of the system Hamiltonian allows us to pose questions concerning the generic behavior of a whole family of systems as opposed to its single realization. Imagine the Hamiltonian of the system is dependent on some parameter λ, $H = H(\lambda)$, and consider the motion of energy levels of the system as λ is varied. The parameter in question may be, for example, the value of the external electric or magnetic field affecting the energy levels of atoms (molecules), as exemplified in studies of the magnetized hydrogen atom [6], the amplitude of the laser (microwave) field leading to ionization (or dissociation) or intermolecular distance in the adiabatic approximation to the molecular Hamiltonian.

One may then define new statistical properties of spectra for a suitable range of λ instead of considering just a single system realization at fixed value of λ, say $\lambda = \lambda_0$. Such measures will not only supplement the statistical information obtained applying the standard RMT for single systems but will provide information about the system studied.

Already in the early days of the study of irregular systems, an increased sensitivity of the energy levels to the small changes of the parameter has been suggested as a signature of the irregular behavior corresponding to the transition from mostly regular to predominantly chaotic classical motion [7, 8]. This sensitivity is closely related to the appearance of multitude of avoided-level crossings (repulsions of adjacent energy levels) [9]. The statistical properties of avoided crossings may be characterized by the probability distribution of gaps, i.e., local minima of the energy difference between the adjacent levels as a function of the parameter varied [10–12]. The detailed analysis of this measure is presented in the paper immediately following this one [13].

The dependence of levels on the small changes of λ may be characterized by the levels curvature $K_n = d^2E_n(\lambda)/d\lambda^2$ [8, 14, 15]. The statistical properties of curvatures have been first discussed in [14, 15]. The authors have derived the expressions for the large-curvature tail of the curvature density distributions, tested them qualitatively on the RMT model, and postulated their universal character. A similar qualitative test of the tail distributions has been performed for the kicked-top model [16] confirming predictions of [15] on the well-known model system exhibiting chaotic dynamics [17–19]. However, a subsequent study [20] has shown that, while the large-curvature tail indeed shows a universal behavior, full-curvature distributions obtained for different systems show significant differences which suggest nonuniversal behavior of small curvatures.

Let us note that, apart from the intrinsic interest in the curvature distribution as one of the statistical measures

of the properties of the levels dependence on the parameter, curvatures, as a second derivative of the energy, are of direct physical importance. The curvature distributions may find direct applications in the description of fluctuations of magnetic (such as the diamagnetic susceptibility [21]) or temperature (e.g., heat capacity) properties in mesoscopic quantum systems or random media.

In this paper we consider several possible distributions describing the generic behavior of curvatures in the whole range of their values. We review in Sec. II, for the sake of completness, the essential points of the statistical approach to curvature distribution as developed by Gaspard *et al.* [14, 15]. This approach enabled the authors [14, 15] to derive the large-curvature tail of the curvature distributions in the limit in which the number of levels N in the system is infinite. The full-curvature distributions seems to be diffucult to evaluate in this limit. A standard approach known from the RMT would be to turn towards the finite-level-number approximation. Such a two-level approach had been quite succesful in the past predicting, e.g., Wigner-type distributions for the nearest-neighbor spacings [1, 2, 4, 5, 22, 23], as well as producing analytic predictions concerning the avoided-crossings distributions [12]. We show, however, that without necessary modifications the fomalism of [14, 15] is unsuitable to treat the finite-N case.

This leads us to reformulating the Gaspard *et al.* [14, 15] theory in a form more suitable for curvature distribution study in finite-dimensional systems (Sec. III). Using a 2×2 theory, we derive expressions for the curvature distributions. By readjusting them to have the same numerical value in the large-curvature limits as the tails of the distribution derived previously [14, 15], we can compare their predictions with numerical data. This provides, at the same time, a quantitative test of the tail distributions. A comparison with numerical data for the kicked-top model shows, however, that the two-level theory, although an improvement over the limiting tail distribution, is not sufficient to reproduce the numerical data satisfactorily. We introduce, therefore, an *ad hoc* solution to the problem, i.e., we present our guess for the curvature distributions—simple analytical function which fit the data for the kicked-top model quite well. In Sec. IV we test, therefore, the proposed expressions on a variety of systems including a generic random-matrix theory model as well as different physical models finding that they reproduce surprisingly accurately the numerical data.

We discuss in detail further the nonuniversal behavior of small curvatures discovered for stadium billiard [20]. We find a similar behavior in the study of the hydrogen atom in a strong magnetic field. Following the original idea [20] we are able to classify qualitatively the degree of "scarring" [24] in different systems studied.

II. CURVATURE DISTRIBUTIONS: $H_1 + \lambda H_2$ DYNAMICS

A. Preliminaries

In this section we shall consider systems for which the Hamilton operator is linearly dependent on the parameter λ,

$$H(\lambda) = H_1 + \lambda H_2, \tag{2.1}$$

where H_1 and H_2 are operators describing some parts of the dynamics. We avoid the standard notation $H = H_0 + \lambda V$, as such a form is frequently used with additional assumptions, e.g., an integrability of the classical equivalent of H_0. We assume that no additional constant of the motion exists. Then the Hamiltonian, Eq. (2.1), may be diagonalized for each λ value by orthogonal, unitary, or symplectic transformation. The type of the transformation necessary for diagonalizing (2.1) classifies the system as belonging to one of the three universality classes known from the RMT [1–5]. The corresponding ensembles of random matrices are called Gaussian orthogonal, unitary, and symplectic ensembles (GOE, GUE, and GSE, respectively).

Recent years have brought numerous examples confirming the conjecture [3] that classically fully chaotic motion is strongly correlated with the fact that the statistical properties of eigenvalues (and eigenvectors) follow predictions of RMT. Throughout this paper we assume, therefore, that (1) classical motion corresponding to the considered $H(\lambda)$ is fully chaotic in the whole interval of λ values, and (2) $H(\lambda)$ belongs to the same universality class in the whole range of λ. We underline that we do not consider the case when a change in λ induces the transition from one universality class to the other as considered, e.g., in [22, 23]. The latter assumption is necessary as it is well known that statistical properties of spectra strongly depend on the universality class the system belongs to. As we shall consider system properties in the whole interval of λ values, we must ensure that within this interval the system behaves in a statistically similar way.

B. Level dynamics and tails of curvature distributions [11]

Consider the motion of eigenvalues of (2.1) treating λ as a fictitious time. It is well known that using the Schrödinger equation

$$H(\lambda)|n,\lambda\rangle = x_n(\lambda)|n,\lambda\rangle, \qquad n = 1, ..., N < \infty \tag{2.2}$$

one may derive [25–28, 4, 15] a set of equations describing the motion of $x_n(\lambda)$ (we follow the notation of [15])

$$\dot{x}_n = p_n, \tag{2.3}$$

$$\dot{p}_n = 2 \sum_{m\ (\neq n)} \frac{L_{nm}L_{mn}}{(x_m - x_n)^3}, \tag{2.4}$$

$$\dot{L}_{mn} = \sum_{l\ (\neq m,n)} L_{ml}L_{ln}[(x_n - x_l)^{-2} - (x_m - x_l)^{-2}], \tag{2.5}$$

where

$$p_n(\lambda) = \langle n,\lambda|H_2|n,\lambda\rangle, \tag{2.6}$$

$$L_{mn}(\lambda) = [x_n(\lambda) - x_m(\lambda)]\langle m,\lambda|H_2|n,\lambda\rangle. \tag{2.7}$$

For all three universality classes L_{mn} may be compactly

represented in the quaternion notation [15]

$$L_{mn}(\lambda) = \sum_{a=0}^{\nu-1} e_a L_{mn}^{(a)}, \tag{2.8}$$

where the index ν takes the following values: $\nu = 1$ for orthogonal, $\nu = 2$ for unitary, and $\nu = 4$ for symplectic systems, respectively. In Eq. (2.8), e_a are unit numbers in the quaternion space, $L_{mn}^{(0)}$ is real antisymmetric, while $L_{mn}^{(a)}$, $a = 1, 2, 3$, are real symmetric with vanishing diagonal elements.

Equations (2.3)–(2.5) may be generated from the classical Hamiltonian [26–28, 15]

$$\mathcal{H}_N = \frac{1}{2}\sum_n p_n^2 + \frac{1}{2}\sum_{\substack{m,n \\ (m\neq n)}} \sum_a \frac{(L_{mn}^{(a)})^2}{(x_m - x_n)^2}, \tag{2.9}$$

assuming appropriate Poisson brackets. Thus an N level parametrically dependent system is equivalent to a set of interacting fictitious particles. The energy levels and their slope with respect to the parameter are identified as positions and momenta of the fictitious particles, respectively. The motion takes place on a manifold of the $[2N + \nu N(N-1)/2]$-dimensional phase space and has been shown [28] to be strictly integrable for any finite N.

An appropriate statistical-mechanics approach to find distributions of different physical quantities would be to define a microcanonical ensemble based on the Hamiltonian, Eq. (2.9), and the appropriate constants of the motion. However, all such independent constants of motion are, as of now, unknown [4]. To avoid this problem a canonical ensemble is constructed [15] restricting the motion of eigenvalues to an interval $[-L/2, L/2]$; at $\pm L/2$ the hard walls are placed. At the end of calculations one lets $L, N \to \infty$ keeping N/L constant. Defining the Gibbs measure

$$dG_{NL} = \frac{1}{Z_{NL}} e^{-\beta \mathcal{H}_N} \prod_{\substack{m,n \\ (1\le m<n\le N)}} \prod_{a=0}^{\nu-1} dx_m dp_m dL_{mn}^{(a)}, \tag{2.10}$$

one finds that β is given by the inverse variance of the Gaussian distribution of velocity p_n [obtained by integrating Eq. (2.10) over all x_i and L_{mn}], while the joint probability density of the energy levels takes the form

$$\rho_{NL}(x_1, ..., x_N) = \frac{1}{\mathcal{N}_{NL}^{\nu}} \prod_{\substack{i,j \\ (1\le i<j\le N)}} |x_i - x_j|^{\nu}. \tag{2.11}$$

In the standard RMT, the joint probability density contains additionally the Gaussian weight function $\exp(-\frac{1}{2}\sum_k x_k^2)$, also the available configuration space is $\mathbb{R}^N$ instead of $[-L/2, L/2]^N$. Yet the authors [15] prove that in the $N, L \to \infty$ limit the characteristic RMT nearest-neighbor spacing distribution for orthogonal and unitary ensembles is recovered taking the average density of states $\bar{\rho} = \frac{2N}{\pi L}$. They conjecture that for the symplectic ensemble their model will also yield the spacing distribution characteristic for GSE. Finally, they consider the distribution of curvatures, i.e., the second derivative of energy levels with respect to the parameter [29]

$$K \equiv \frac{d^2 x_n}{d\lambda^2} \tag{2.12}$$

and find that the large curvature tails of the distributions are given by

$$P_O(K) = \frac{\pi^2}{2}\left(\frac{\bar{\rho}}{\beta}\right)^2 |K|^{-3} + \cdots, \tag{2.13}$$

$$P_U(K) = 2^4\pi^2\left(\frac{\bar{\rho}}{\beta}\right)^3 |K|^{-4} + \cdots, \tag{2.14}$$

$$P_S(K) = \frac{2^{13}\pi^4}{3}\left(\frac{\bar{\rho}}{\beta}\right)^5 |K|^{-6} + \cdots, \tag{2.15}$$

for GOE, GUE, and GSE, respectively.

The expressions (2.13)–(2.15) have been compared with numerical experiments resulting from the random-matrix model [15] as well as with data obtained for various physical systems [16, 20]. In all these studies, however, only the slope of the tail distributions (2.13)–(2.15) has been tested, and no attention has been paid to the coefficients appearing in the formulas. One of the aims of this paper is to fill this gap.

At the same time we find that the lack of even some approximate formulas for the full curvature distribution is highly unsatisfactory. Unfortunately, we were also unable to obtain such expressions from the formalism sketched above. It is well known [1–5] that approximate level-spacing distributions may be obtained in the RMT by considering a simple two-level model system. The resulting so-called Wigner surmise formulas approximate very well the level-spacing distributions for arbitrary-N systems. In an attempt to derive an analytic approximation for the curvature distribution a natural first step would be to consider, therefore, the $N = 2$ model within the theory of [14, 15]. However, immediately one is faced with a serious difficulty. Not only the two-level theory but also any finite-N-level theory must fail in predicting the small-curvature behavior for the assumed linear dependence of the Hamiltonian, Eq. (2.1), on the parameter λ. In such a theory no limits on λ values are imposed. One immediately notices that for very large λ values the H_1 part is negligible and the eigenvalues are essentially that of H_2 multiplied by λ. Their curvatures will be very small for such λ values. The origin of this behavior lies in the fact that for the assumed linear dependence in λ, the "gas" of particles—levels described by the Hamiltonian (2.9)—expands indefinitely. This means that the statistical properties of energy levels are not stationary when λ varies, preventing the system from reaching a thermodynamic equilibrium. The Gibbs measure, Eq. (2.10) is thus clearly inadequate. To remedy this unpleasant situation Gaspard *et al.* [15] have put hard walls in their model (see above) but then they could recover RMT predictions, e.g., for the level spacings in the limit of $N = \infty$ only. For any finite N their theory does not reproduce the corresponding RMT predictions.

In our opinion a more satisfactory solution to this problem is presented in the next section.

III. ALTERNATIVE LEVEL DYNAMICS

A. Formulation of the problem

To remedy the "expansion problem" of the "gas of levels" one may assume a different from (2.1) dependence of the Hamiltonian on the parameter λ. This problem has been studied in detail in [4]. Assuming that this dependence takes a quite general form

$$H = f(\lambda)H_1 + g(\lambda)H_2. \tag{3.1}$$

and requiring the levels motion to be again equivalent to the classical motion of a fictitious many-particle systems restricts the admissible $f(\lambda)$ and $g(\lambda)$; see [4] for details. In fact, a quite nice choice is realized assuming the form

$$H = \cos(\lambda)H_1 + \sin(\lambda)H_2. \tag{3.2}$$

If H_1 and H_2 are two random matrices of the same RMT ensemble (GOE, GUE, or GSE), the above choice ensures the stationarity (with respect to λ) of the statistical properties of energy levels (density of states, spacing distribution, slopes, etc.) which strongly supports the thermodynamic approach to the problem. The definition, Eq. (3.2), is equivalent to the linear λ-dependence model of the previous system for λ small. The corresponding classical Hamiltonian for the fictitious interacting particles reads

$$\mathcal{H}_N = \frac{1}{2}\sum_n (p_n^2 + x_n^2) + \frac{1}{2}\sum_{\substack{m,n \\ (m\neq n)}}\sum_a \frac{(L_{mn}^{(a)})^2}{(x_m - x_n)^2}, \tag{3.3}$$

where L_{mn} now differs from (2.7) by division by $\cos(\lambda)$,

$$L_{mn}(\lambda) = \frac{[x_n(\lambda) - x_m(\lambda)]\langle m, \lambda|H_2|n, \lambda\rangle}{\cos(\lambda)}. \tag{3.4}$$

The Hamiltonian, Eq. (3.3), differs from Eq. (2.9) by the presence of the additional harmonic well which binds the particles (levels) together preventing them from flying apart. We call the model defined by Eq. (3.3) the "contained gas" in contrast to the "expanding gas" defined by Eq. (2.9) [31]. Using the same Poisson brackets [15, 4] as before, the equations of motion are obtained. They take the same form as Eqs. (2.3)–(2.5), except that the force equation contains now additional term coming from the binding potential

$$\dot{p}_n = -x_n + 2\sum_{m\ (\neq n)} \frac{L_{nm}L_{mn}}{(x_m - x_n)^3}. \tag{3.5}$$

The nicest thing about the level dynamics corresponding to (3.3) comes when, following [15], we attempt to construct the appropriate canonical ensemble. Using the Gibbs measure

$$dG_N = \frac{1}{Z_N} e^{-\beta\mathcal{H}_N} \prod_{\substack{m,n \\ (1\leq m<n\leq N)}} \prod_{a=0}^{\nu-1} dx_m dp_m dL_{mn}^{(a)} \tag{3.6}$$

[with $\mathcal{H}_N$ given now by Eq. (3.3)] one obtains the joint probability density for the energy levels in the form

$$\rho_N(x_1, ..., x_N) = \frac{1}{\mathcal{N}_N^\nu} \exp\left(-\frac{\beta}{2}\sum_k x_k^2\right) \prod_{\substack{i,j \\ (1\leq i<j\leq N)}} |x_i - x_j|^\nu \tag{3.7}$$

yielding the RMT joint probability density for arbitrary N value. Therefore the statistical mechanics for the contained gas leads to RMT for arbitrary N [4]. In particular, for the $N = 2$ level model, (3.7) yields immediately the Wigner level spacing formula, Eq. (4.13), with $\sigma = \beta^{-1/2}$. For different N, other values of β lead to a unit average spacing. In the large-N limit one recovers from Eq. (3.7) the Wigner semicircle law for the ensemble-average level density $\bar{\rho}(x)$ following standard derivations of RMT [1, 4]

$$\bar{\rho}(x) = \frac{\beta}{\pi\nu}\left(\frac{2N\nu}{\beta} - x^2\right)^{1/2}. \tag{3.8}$$

It shows clearly that, in the model considered here, there is only one parameter β, which determines the average level density, i.e., the mean spacing. This makes a minor difference as compared with the model considered in [15] (see Sec. II B), since the replacement of $\cos(\lambda)$ [$\sin(\lambda)$] by $\cos(a\lambda)$ [$\sin(a\lambda)$] in Eq. (3.2) allows us immediately to obtain two independent quantities $\bar{\rho}$ and β.

As in the expanding-gas model, Eq. (3.6) yields the Gaussian normal distribution with zero mean and the variance β^{-1} for the velocity distribution by straighforward integration of Eq. (3.7) over all x_m, $L_{mn}^{(a)}$, and all but one momenta (velocities) p_m.

Consider now the curvature distribution. It is easy to notice that in the asymptotic $N \to \infty$ limit the canonical ensemble for both the expanding gas, Eq. (2.9), considered in [15] and the contained gas, Eq. (3.3), will lead the same predictions concerning the distributions of curvatures and, in particular, to the same large curvature tails given by Eqs. (2.13)–(2.15) (provided the average level density $\bar{\rho}$ is determined from β for the contained gas), similarly to the nearest spacing distributions as proved in [15]. The advantage of the presently considered model lies in the possibility of using the finite-N theory in an attempt to obtain predictions concerning full-curvature distributions and not merely the large-curvature tails of them. Here we shall consider the $N = 2$ case only as we have been unable (although we have not lost the hope yet) to solve the problem in the general case.

B. Curvature distributions in the $N = 2$ model

Before presenting the calculations for the two-level model, it is worth clarifying one point, already mentioned in Sec. III A, i.e., applicability of the canonical ensemble with the Gibbs measure, Eq. (3.6). In the $N = 2$ case, it is easy to find all necessary integrals of motion to treat correctly the two-level model using the microcanonical ensemble. In particular, note that for the GOE case the $L_{12}^{(0)}$ is then the constant of motion. Were the two-level system completely isolated, the microcanonical ensemble would be a proper choice. The application of the canonical ensemble, on the other hand, is equivalent to a more

realistic assumption that the two-level system weakly interacts with the remaining levels. We do not expect that the curvature distributions obtained in this simple model will work so well as for the level-spacing distributions or for the avoided-crossing distribution [12, 13]. Due to the long range of the potential in Eq. (3.3), for small curvatures one expects the $N = 2$ model to produce results different from those expected in the large-N limit. On the other hand, the two-level approximation should work quite well in the limit of large curvatures, where an interaction of two adjacent levels close to the avoided crossing should be dominant.

The curvature distribution for the $N = 2$ case, using Eqs. (3.5) and (3.6), is

$$P(K) = \int dG_2 \delta \left(K + x_1 - 2 \sum_{a=0}^{\nu-1} \frac{(L_{12}^{(a)})^2}{(x_1 - x_2)^3} \right). \tag{3.9}$$

The Gaussian integrals over momenta in (3.9) are carried out first. Next we take care of the δ function by integrating over one of the $L_{12}^{(a)}$, say $L_{12}^{(0)}$. Consider first, in more detail, the GOE $\nu = 1$ case. The resulting integral may be put in the form [after determining separately the normalization factor Z_2 in Eq. (3.6)]

$$P_O(K) = \frac{3\beta^{3/4}}{16\sqrt{2\pi}} [\mathcal{I}_O(K) + \mathcal{I}_O(-K)], \tag{3.10}$$

which makes the symmetry of the distribution with respect to $K = 0$ apparent. The function $\mathcal{I}_O(K)$ may be expressed as

$$\mathcal{I}_O(K) = \int_0^\infty dx x^{-1/2} \exp[-\beta(x - K)^2)] \times \mathcal{D}_{-5/2} \left(\frac{\sqrt{\beta}}{2} (2K - x) \right), \tag{3.11}$$

where the $\mathcal{D}_p(z)$ is shorthand notation for the product of a parabolic cylinder function $D_p(z)$ [30] with an exponential

$$\mathcal{D}_p(z) = \exp(z^2/4) D_p(z). \tag{3.12}$$

Using the asymptotic form for $D_p(z)$ [30] we get for $\mathcal{D}_p(z)$ in the limit of large z

$$\mathcal{D}_p(z) \propto z^p [1 + O(z^{-2})]. \tag{3.13}$$

We were not able to reduce (3.17) further. For large K, the dominant part of the integral comes from $x \approx K$. Together with the asymptotic form (3.13) one obtains for the large-$|K|$ limit

$$P_O(K) = \frac{3}{4\beta} \frac{1}{|K|^3} + \cdots . \tag{3.14}$$

The above formula has to be reexpressed in terms of the average density of states $\bar{\rho}$ in order to compare with the tail distribution, Eq. (2.13). The average level density for $N = 2$ case differs significantly from the Wigner semicircle law being explicitly given by

$$\bar{\rho}_2(x) = \sqrt{\frac{\beta}{\pi}} \exp\left(-\frac{\beta}{2} x^2 \right) \times \left[\exp\left(-\frac{\beta}{2} x^2 \right) + \sqrt{\frac{\pi\beta}{2}} x \operatorname{erf}\left(\sqrt{\frac{\beta}{2}} x \right) \right], \tag{3.15}$$

with $\operatorname{erf}(x)$ being the error function. As $\bar{\rho}_2(x)$ is not approximately constant over the region of interest it is difficult to define the average density of states. To avoid this problem we have chosen to adjust $\bar{\rho}$ to fit the correct long tail distribution, Eq. (2.13). This leads to

$$P_O(K) = \frac{3}{16\sqrt{2\pi A^3}} [\mathcal{I}_O(K) + \mathcal{I}_O(-K)] \tag{3.16}$$

with $\mathcal{I}_O(K)$ reexpressed as

$$\mathcal{I}_O(K) = \int_0^\infty dx x^{-1/2} \exp[-(x - K)^2/A^2] \times \mathcal{D}_{-5/2} \left(\frac{2K - x}{2A} \right) \tag{3.17}$$

and with

$$A = \sqrt{\frac{2}{3}} \frac{\pi\bar{\rho}}{\beta}. \tag{3.18}$$

The distributions for the GUE and the GSE cases are derived in quite an analogous way. After a similar fitting (performed for the same reason) one obtains

$$P_U(K) = \frac{3}{4\pi A^2} [\mathcal{I}_U(K) + \mathcal{I}_U(-K)] \tag{3.19}$$

with

$$\mathcal{I}_U(K) = \int_0^\infty dx \exp[-(x - K)^2/A^2] \mathcal{D}_{-4} \left(\frac{2K - x}{2A} \right). \tag{3.20}$$

A comparison of Eq. (2.14) with the limit of large K of Eq. (3.19) yields

$$A = \frac{4^{1/3}\pi^{5/6}}{3^{1/3}} \frac{\bar{\rho}}{\beta}. \tag{3.21}$$

The $P_U(K)$ [Eq. (3.19)] may be expressed in another form by reversing the order of integration. The new final expression is an integral of the polynomial, exponential, and the error function which we were not able to reduce further. For consistency with other formulas, we have chosen here the representation given by Eq. (3.19).

The corresponding expressions for GSE case are

$$P_S(K) = \frac{15}{2\pi A^3} [\mathcal{I}_S(K) + \mathcal{I}_S(-K)] \tag{3.22}$$

with

$$\mathcal{I}_S(K) = \int_0^\infty dx x \exp[-(x - K)^2/A^2] \mathcal{D}_{-7} \left(\frac{2K - x}{2A} \right). \tag{3.23}$$

A comparison of (2.15) with the limit of large K of (3.22) yields

$$A = \left(\frac{2^7\pi^{9/2}}{45}\right)^{1/5}\frac{\rho}{\beta}. \tag{3.24}$$

The tests of the distributions given by Eqs. (3.16), (3.19), and (3.22) have been performed by comparison with the numerical data for the kicked-top model [17–19]. The resulting dynamics belongs to the circular rather than Gaussian ensembles [4], as the system studied belongs to a class of periodically perturbed models for which the Hamiltonian reads

$$H = H_0 + \lambda V f(t), \quad f(t) = \sum_{n=-\infty}^{\infty}\delta(t-n). \tag{3.25}$$

Here the eigenphases of the unitary operator describing the evolution over one period

$$U = e^{-iH_0}e^{-iV} \tag{3.26}$$

play the role of eigenvalues in statistical analysis. Several previous studies (see [17–19], a more complete list of references may be found in [4]) have shown that this model is very faithful to the RMT predictions which, e.g., level spacings do not distinguish between circular and Gaussian ensembles. For this system all three universality classes may be realized by a proper choice of H_0 and V and, importantly, the curvature data have been kindly supplied to us by the authors [16].

In the original publication [16] only a qualitative comparison of predicted slopes [Eqs. (2.13)–(2.15)] with numerical histograms has been made. The average density of states is $\bar{\rho} = N/2\pi$ and the parameter β is extracted from the numerically computed velocity distribution (for the parameters of [16]), which turned out to be well approximated by a Gaussian ensemble. This provided a test that indeed the theory of [15] should be applicable.

The comparison of the theory and numerical experiment is presented in Figs. 1–3 for the orthogonal, unitary, and symplectic cases, respectively. The numerical histograms are taken from [16] (see this reference for details on the model and parameter values), dotted lines give the long tail prediction of [15], while solid lines represent Eqs. (3.16), (3.19), and (3.22), respectively. We would like to stress that no free parameters enter into this calculation.

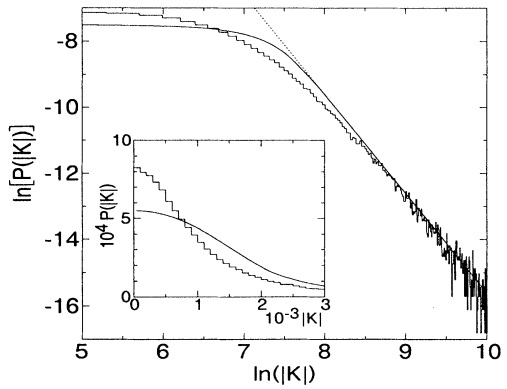

FIG. 1. Normalized curvature histogram compared with the tail prediction (2.13) (dotted line) and the approximate distribution (3.16) in the log-log scale for the orthogonal kicked-top model. The inset shows the small-curvature behavior in the linear scale. Numerical data for curvatures obtained by courtesy of F. Haake and D. Saher. For further details see text.

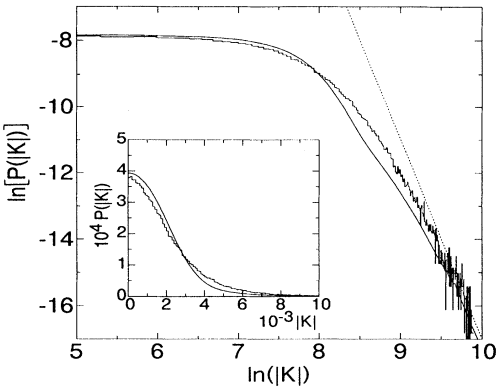

FIG. 2. Same as Fig. 1 but for the unitary kicked top. The comparison is made with the distribution given by Eq. (3.19). For details see text.

For the large-curvature limit the comparison of the data with dotted lines show quite good agreement between numerical data and the theory, Eqs. (2.13)–(2.15) [15]. Let us stress that this provides a quantitative test of this theory. Note that while in the orthogonal case (Fig. 1) the large-curvature limit is really reached as indicated by a coalescing dotted and solid lines, this is not completely the case for both unitary (Fig. 2) and symplectic (Fig. 3) cases. The agreement at low curvatures is not good, as anticipated, and is shown in the insets to the figures. The agreement becomes slightly better with increasing ν, i.e., going from orthogonal to the symplectic class but certainly is far from being satisfactory.

We must stress that the distributions found above are quite difficult to compute numerically, especially for large values of K/A. We could not find an available routine for

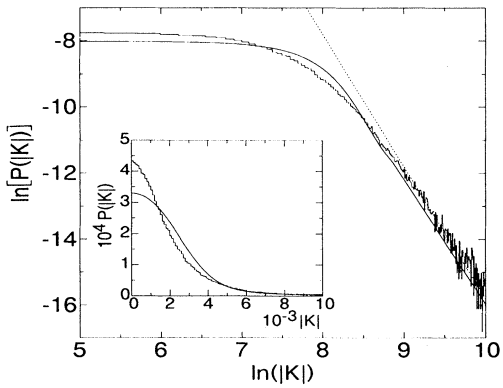

FIG. 3. Same as Fig. 1 but for the symplectic kicked top. The comparison is made with the distribution given by Eq. (3.22). For details see text.

the parabolic cylinder function $D_p(x)$ working reliably for arbitrary x and negative p. To evaluate this function, or rather the function $\mathcal{D}_p(x)$ defined previously in Eq. (3.12), we have combined the series expansion valid for small x with the asymptotic expansion [of which the leading term is given by Eq. (3.13)] valid for large x. We believe that the "theoretical" curves in Figs. 1–3 are accurate to within the 1% relative accuracy. Let us also note that for negative integer p, $\mathcal{D}_p(x)$ is expressible in terms of exponentials and error functions. This expansion, however, at least in double precision arithmetics, fails even for moderate values of K/A.

Clearly, to get a better approximation for the curvature distribution one needs to go beyond the two-level approximation and consider either the $N = \infty$ model of [15] or, which may be technically simpler, start from the finite-N-level contained gas model for N large. Let us stress again that this necessity is due to the long ranging potential in Hamiltonians (2.9) and (3.3).

Unfortunately, as mentioned before, this problem still awaits a rigorous solution. Being unable to perform the required calculation, we have been left with the only possible other solution to the problem, i.e., to *guess* the appropriate formulas.

C. A guess for the curvature distributions

The guess we present below is based on the only accurate prediction available [15], i.e., the tail distribution formulas given by Eqs. (2.13)–(2.15). We require also, as for every good guess, that the resulting formulas should be as simple as possible. The simplest form we could think of takes the form of the Lorentzian function taken to the appropriate power to ensure proper limiting behavior for large $|K|$. Thus we have

$$P(K) = \mathcal{N}_\nu \frac{1}{[1 + (K/\gamma_\nu)^2]^{(\nu+2)/2}} \tag{3.27}$$

(with, as usual, $\nu = 1, 2, 4$ for GOE, GUE, and GSE, respectively). Defining the dimensionless curvature k as

$$k = \frac{K}{\gamma_\nu}, \tag{3.28}$$

we have explicitly

$$P_O(K) = \frac{1}{2}\frac{1}{(1+k^2)^{3/2}}, \tag{3.29}$$

$$P_U(K) = \frac{2}{\pi}\frac{1}{(1+k^2)^2}, \tag{3.30}$$

$$P_S(K) = \frac{8}{3\pi}\frac{1}{(1+k^2)^3}. \tag{3.31}$$

The first remarkable finding occurs when we compare the large curvature behavior of Eqs. (3.29)–(3.31) with the exact tail distributions Eqs. (2.13)–(2.15). We obtain

$$\gamma_O = \pi\frac{\bar{\rho}}{\beta} \tag{3.32}$$

for the GOE,

$$\gamma_U = 2\pi\frac{\bar{\rho}}{\beta} \tag{3.33}$$

for the GUE, and

$$\gamma_S = 4\pi\frac{\bar{\rho}}{\beta} \tag{3.34}$$

for the GSE. Clearly, despite the fact that the coefficients in Eqs. (2.13)–(2.15) are quite complicated, quite surprisingly a single relation links γ with the $\bar{\rho}/\beta$ ratio for all three universality classes, namely

$$\gamma_\nu = \nu\pi\frac{\bar{\rho}}{\beta}, \tag{3.35}$$

where $\nu = 1, 2, 4$ for GOE, GUE, and GSE, the same ν which, e.g., determines the degree of level repulsion.

In describing the curvature distributions for a generic quantum system, the problems with the present model are similar to that encountered with direct application of RMT to the nearest-neighbor level-spacing distribution [1–5], i.e., the real systems do not obey the semicircle law. Rather, one can assume locally that the level spacing is uniform. For the real system, therefore, β and $\bar{\rho}$ have to be separately determined. In this context, the tail formulas, Eqs. (2.13)–(2.15), coming from the model of [15] are useful in applications to fix the $\bar{\rho}/\beta$ ratio and thus γ_ν. Examples of such a situation are given below and in Sec. IV.

The truly amazing fact appears when one compares the distributions (3.29)–(3.31) with numerical data for kicked top as shown in Figs. 4–6 for the orthogonal, unitary, and symplectic cases, respectively. The insets in the figures show the detail of the small-curvature distribution in the linear scale. Recall that $\bar{\rho}$ and β are determined independently. For each universality class, γ is calculated using Eq. (3.35) from available $\bar{\rho}$ and β, no fit is being performed. This time, the agreement between the data and the guessed distributions is quite good for all three universality classes. Note the deviations from

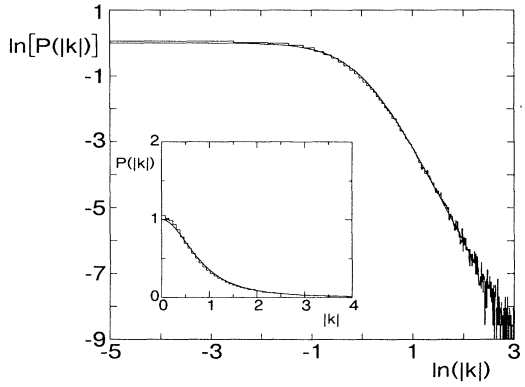

FIG. 4. Same as Fig. 1 except the comparison is made with the distribution given by Eq. (3.29). The inset shows the small-curvature behavior in the linear scale. Note the change of horizontal and vertical scales in comparison to preceding figures—the dimensionless curvature is used and no rescaling of the data for the linear plot in the inset is necessary.

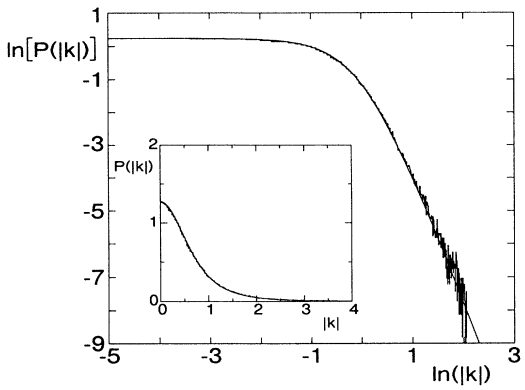

FIG. 5. Same as Fig. 4 but for the unitary kicked top. The comparison is made with the distribution given by Eq. (3.30). The same scale as in Fig. 4. For details see text.

the "ad hoc" distributions predictions for the orthogonal and especially symplectic cases. We shall return to this point later while discussing the nonuniversality of small-curvature distribution.

Certainly, a single comparison with data originating from one model, even as celebrated as the kicked top, should not allow us to draw any definite conclusions. After all, it has been shown that the small-curvature behavior may be system dependent [20] and, therefore the agreement obtained may be just a coincidence. To check whether this is not the case, we have to compare the distributions (3.29)–(3.31) with numerical data coming from other physical models as well as with that originating from the genuine random dynamics. Such a comparison is the object of the next section.

IV. OTHER SYSTEMS

A. Random model

As a first example of this section let us consider a parametric motion of levels in a random system. We define

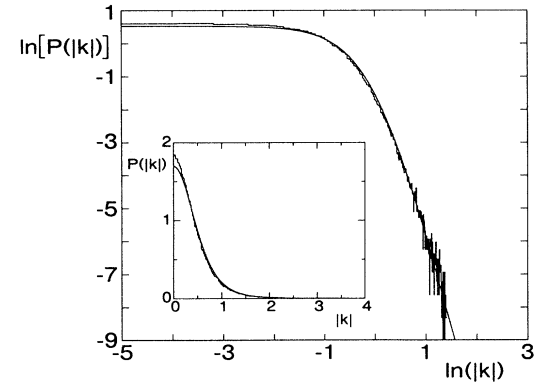

FIG. 6. Same as Fig. 4 but for the symplectic kicked top. The comparison is made with the distribution given by Eq. (3.31).

the random Hamiltonian matrix in a form of Eq. (3.2),

$$H(\lambda) = \cos(\lambda)H_1 + \sin(\lambda)H_2, \tag{4.1}$$

repeated here for convenience. It is apparent that the maximal interval leading to independent dynamics is now restricted to $\lambda \in [0, \pi)$, while the dynamics changes from that determined by H_1 to the one dominated by H_2 in $[0, \pi/2]$ interval. The "random" dynamics is generated by an appropriate choice of matrices H_1 and H_2. For a considered universality class we assume that both H_1 and H_2 belong to this class [so in the whole interval of λ values, $H(\lambda)$ belongs to the same universality class].

Numerically H_i are generated according to prescription given, e.g., in [5]. Let S (A) denotes a real symmetric (antisymmetric) matrix (of dimension $N \times N$). Then, explicitly

$$(\nu = 1) \qquad H_i = S \tag{4.2}$$

$$(\nu = 2) \qquad H_i = S + iA \tag{4.3}$$

$$(\nu = 4) \qquad H_i = Se_0 + A^1 e_1 + A^2 e_2 + A^3 e_3, \tag{4.4}$$

where e_i are 2×2 matrix representation of quaternion unit numbers:

$$e_0 = \begin{pmatrix} 1 & 0 \\ 0 & 1 \end{pmatrix}, \qquad e_1 = \begin{pmatrix} 0 & i \\ i & 0 \end{pmatrix},$$

$$e_2 = \begin{pmatrix} 0 & -1 \\ 1 & 0 \end{pmatrix}, \qquad e_3 = \begin{pmatrix} i & 0 \\ 0 & -i \end{pmatrix}, \tag{4.5}$$

and the direct product of matrices in Eq. (4.4) is assumed. The independent matrix elements of symmetric matrices are generated from the zero-centered normal distribution with the variance for the diagonal elements being twice the variance for the nondiagonal elements

$$\bar{S_{ij}^2} = (1 + \delta_{ij})\frac{1}{2\beta}, \quad i \le j \tag{4.6}$$

and the elements of antisymmetric matrices are also zero-centered normally distributed with the same variance $2/\beta$, having obviously zero on the diagonal. The assumed form of the Hamiltonian $H(\lambda)$ in Eq. (4.1) ensures that the density of states for different λ values are the same and, moreover, the joint probability density at each λ value takes the form of Eq. (3.7).

The numerical results have been obtained in the following way. Matrices H_i have been generated as described above. The resulting Hamiltonian $H(\lambda)$ has been diagonalized for different values of $\lambda \in [0, \pi/2)$. The step in λ has been chosen sufficiently small to allow us to obtain the velocities (first derivative with respect to λ) and the curvatures of the levels (i.e., their second derivative with respect to λ) approximated by the finite difference. Both velocities and curvatures have been calculated at λ values sufficiently separated to make them reasonably statistically independent. To obtain statistically convincing samples, several random H_1 and H_2 choices have been used. The additional averaging makes the results independent of any single realization of matrices H_i.

The produced data allow us to test two important conjectures made previously. First, as noted several times

above, the canonical ensemble is not, strictly speaking, the appropriate choice due to the integrability of the fictitious-particle Hamiltonian, Eq. (3.3). The proper choice should be the microcanonical ensemble. We can, at least partially, test the canonical ensemble approximation by comparing its predictions, e.g., concerning the velocity distribution with numerical results. Second, we may compare the *ad hoc* assumed distributions of curvatures Eq. (3.27) with numerical data for a genuine random model.

The data have been obtained for $N = 200$ matrices for the variance of the matrix elements of H_i in Eq. (4.6)

$$\frac{1}{2\beta} = \frac{1}{4N\nu}, \tag{4.7}$$

i.e., $\beta = 2N\nu$. Equation (3.8) then reduces to

$$\bar{\rho}(x) = \frac{2N}{\pi}(1 - x^2)^{1/2}, \tag{4.8}$$

which indeed is reproduced very well by the numerically simulated density of levels.

As mentioned in Sec. III, the canonical ensemble defined by Eq. (3.6) predicts a Gaussian velocity distribution with zero mean and the variance β^{-1}. We have found numerically the velocity distribution and its variance. To stay in the "flat maximum" interval of the semicircle, only the velocities of levels lying in the interval $[-0.4, 0.4]$ were taken for the analysis.

Indeed, the velocity distributions for all three universality classes are approximated very well by Gaussian distributions of zero mean (the results are plotted in [13] where some additional tests are made). The variances obtained directly numerically (and not from the fit to Gaussian distributions) are equal to 401, 805, and 1616 as compared with theoretical values of 400, 800, and 1600. This is quite good agreement (about 20 000 velocities were taken for each average).

Let us concentrate in more detail on the curvature distributions. Curvatures were obtained from the finite-difference approximation based on three consecutive diagonalization with a very small step in λ. Next, λ was increased by a much larger amount to the next point around which curvatures were calculated. Relatively large spacing between values at which curvatures have been found should minimize correlations between results of different triple diagonalizations. As mentioned above, several random matrices H_1 and H_2 were used to average over their individual realizations. Only the curvatures of levels lying in the $[-0.4, 0.4]$ interval were collected. The average density of states, needed to determine γ_ν, was obtained by averaging the semicircle law Eq. (4.8) over the interval of x values taken for the analysis. For each universality class the numerically obtained velocity variance has been used in Eq. (3.35). The total number of curvatures used in the final plots, presented in Figs. 7 (the linear scale) and 8 (the logaritmic scale) was about 198 000 curvatures per universality class. Note that this time the agreement between the *ad hoc* distributions Eq. (3.27) and the numerical data is such an excellent one that it is hard to notice the theoretical curves under the histograms. This result speaks for itself and provides the strong support for our guessed distributions Eq. (3.27). Note also nice agreement in the tail distribution, which provides further quantitative agreement with Eqs. (2.13)–(2.15) of [15].

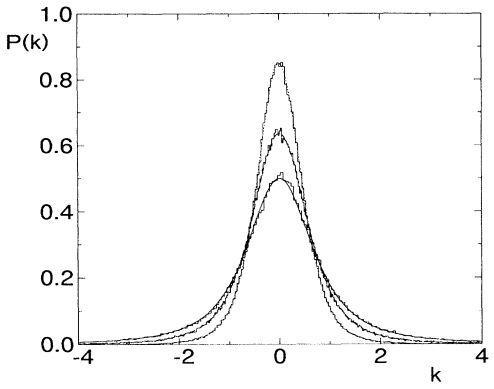

FIG. 7. The normalized curvature histograms for the random dynamics model for all three universality classes. The corresponding *ad hoc* distributions are drawn by solid, dashed, and dotted lines for GOE, GUE, and GSE, respectively. For a discussion see text.

B. Kicked rotator and stadium billiard

The curvature distributions for the kicked-rotator model has been studied by Takami and Hasegawa [20]. The authors were most kind to make their data available to us for comparison with theoretical distributions. After appropriately rescaling their data to our definition of dimensionless curvature k, Eq. (3.28) [32], we compare them with the predictions given by Eqs. (3.29) and (3.30), respectively (for the description of the kicked-rotator model and the values of parameters see [20]).

Figure 9 shows the curvature distribution for the orthogonal kicked-rotator case in the logaritmic scale together with the theoretical curve, Eq. (3.29). No fitting has been done and the agreement for large curvatures with the tail of the distribution is quite good. The scale is chosen such that it coincides with the scale of Figs. 4–7

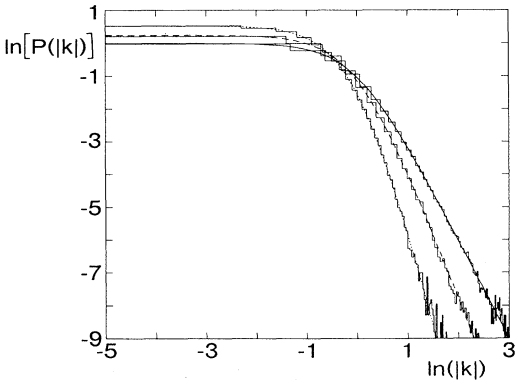

FIG. 8. Same as Fig. 7 but in the logarithmic scale showing agreement in the large-k limit.

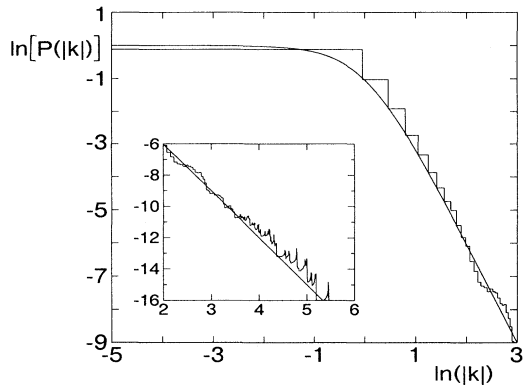

FIG. 9. Comparison of the theoretical *ad hoc* distribution with the curvature distribution obtained for the orthogonal kicked rotator. Data obtained by courtesy of T. Takami and H. Hasegawa. The inset shows very-large-curvature behavior, the axes of the inset match the axes of the main figure, so their title in the inset is suppressed for clarity. For a discussion see text.

for better comparison. Once more, therefore, a quantitative test of Eq. (2.13) confirms this formula. The inset shows even larger curvatures (the slope of the line is different due to different scale). One notices a small deviation from the linear (with slope $p = -3$) behavior for very large curvatures—in this regime, however, the number of data points was probably too low. Notice also significant asymmetric peaks. Local maxima of curvatures are obtained in the vicinity of narrow avoided crossings. If the step in determining the curvatures is very low, then one will obtain contributions from a single level to each bin consecutively up to the locally maximal curvature at the crossing. This characteristic behavior indicates, therefore, that the data points are not statistically independent, at least for very large curvatures.

A proper comparison with the distribution Eq. (3.29) should be, however, made also in linear scale for the study of small-curvature behavior. The results, following Takami and Hasegawa [20] are presented in Fig. 10.

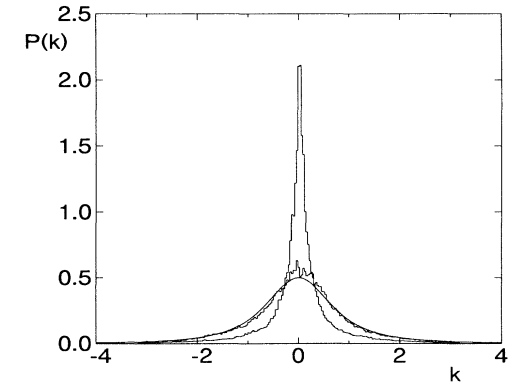

FIG. 10. Small-curvature distribution for the stadium billiard and the orthogonal kicked rotator (data courtesy of T. Takami and H. Hasegawa). For comparison the *ad hoc* theoretical distribution is also drawn as a smooth line.

The figure contains also the data (appropriately rescaled [32]) for the stadium, obtained also from Takami and Hasegawa. One notes that the distribution given by Eq. (3.29) quite correctly describes the behavior of the kicked-rotator curvatures, except for a small excess in numerical data in the vicinity of $k = 0$. By comparison, the data for the stadium billiard yield, as found in [20], completely different distribution at small curvatures. As pointed out by Takami and Hasegawa, this indicates the nonuniversal small-curvature behavior and has been related by them to the abundance of strongly scarred states [24] in the system. These states shift in energy almost linearly with the change of the parameter (here, the aspect ratio of the radius of the semicirle part to the length of the straight part in the stadium) except when they undergo a small avoided crossing.

The large-curvature behavior in the stadium-billiard case is studied in Fig. 11. A comparison with the limiting behavior given by Eq. (2.13) shows that this time the large-k limit behavior is *not* given by the k^{-3} dependence. This behavior has not been noticed in [20] as there only a qualitative comparison has been made. We will come back to this point in more detail after presenting the results for the magnetized hydrogen atom.

Figure 12 shows the curvature distribution for the unitary kicked rotator in comparison with the Eq. (3.30) distribution. The results provide evidence of the correctness of both the tail distribution and formula Eq. (3.30) for the full curvature distribution.

C. Magnetized hydrogen atom

As a final example let us consider one of the most prominent systems of "quantum chaos"—the hydrogen atom in a strong uniform magnetic field. For the review of its properties see recent reviews [6, 33]. The Hamiltonian of the hydrogen atom placed in a static uniform magnetic field, after omitting the trivial Zeeman term, reads in atomic units

$$H = \frac{p^2}{2} - \frac{1}{r} + \frac{B^2}{8}\left(x^2 + y^2\right). \tag{4.9}$$

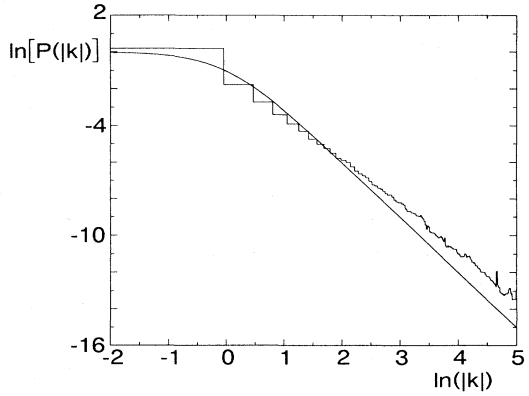

FIG. 11. Large-curvature behavior of the stadium billiard curvatures in the logarithmic scale (data courtesy of T. Takami and H. Hasegawa). Note the deviation from the theoretical distribution, in particular, the difference in the limit slope.

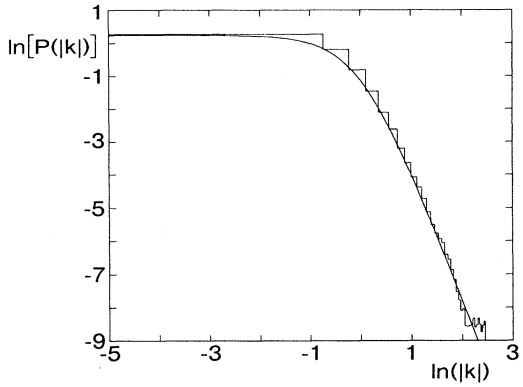

FIG. 12. Large-curvature behavior of the unitary kicked rotator in comparison with the theoretical *ad hoc* distribution. Note quite an excellent agreement in striking contrast to Fig. 11. Data courtesy of T. Takami and H. Hasegawa.

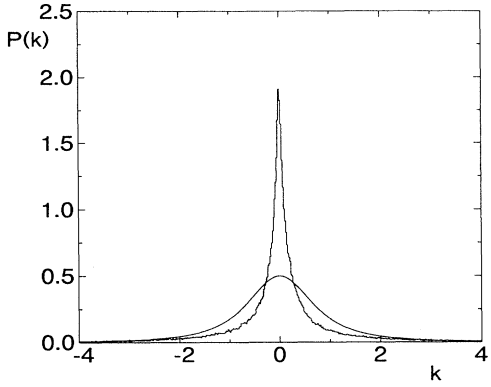

FIG. 13. "Nonuniversal" behavior of small-curvature distribution for the magnetized hydrogen atom. Smooth line represents the *ad hoc* theoretical distribution. More than 140 000 curvatures have been used to obtain the normalized histogram.

It has been shown frequently in the past (see [6] for review and the extensive list of references to original papers) that the classical behavior of the system is determined by the so-called scaled energy $\varepsilon = E/B^{2/3}$, where E is the energy corresponding to Hamiltonian (4.9). For $\varepsilon \geq -0.127$ the classical motion is predominantly chaotic. Instead of diagonalizing the Hamiltonian (4.9), it is advantageous to rewrite the Schrödinger equation in the semiparabolic coordinates treating ε as a parameter and obtaining as eigenvalues the quantized values of the magnetic field or, as it may be better expressed, for fixed both the energy and the magnetic field one finds the spectrum of $\hbar$, i.e., the values of $\hbar$ for which an eigenstate with energy E and the field value B exists [6].

To find the curvatures, the Hamiltonian of the system in semiparabolic coordinates is diagonalized for different $\varepsilon \in (-0.125, -0.075)$ values. The Lanczos algorithm, used for diagonalizations, produces both the eigenvalues and the eigenvectors in the prescribed eigenvalue range. The eigenvectors are used to obtain the slopes p_n [compare Eq. (2.6)]. Two diagonalizations closely spaced in ε give us about 300 curvatures using the first-order finite-difference method as applied to the slopes found (levels from around 250th to around 550th are used). Then ε is increased in value and the procedure is repeated. The relatively large spacing between consecutive double diagonalization is intended to minimize statistical correlations between different sets of curvatures. We have checked that the level spacing is well represented by the Wigner surmise in agreement with previous studies in this regime [6]. Altogether more than 140 000 curvatures have been collected in this way.

The numerically obtained curvature distribution, together with the distribution given by Eq. (3.29), is shown in Fig. 13 in the linear scale and in Fig. 14 in the logaritmic scale. Immediately one notices a huge similarity of the numerical curvature distribution for the magnetized hydrogen atom to the behavior observed for the stadium billiard. Both distributions are strikingly similar, especially for small curvatures. The deviation from the anticipated large-k behavior is, however, much smaller for the magnetized hydrogen atom (Fig. 14). In our case the slope seems to behave according to the k^{-3} rule, and the line in the logarithmic plot appears to be shifted with respect to the data.

To find the origin of the deviation from the tail expression Eq. (2.13) for the large curvatures we have checked whether the other basic results of the theory [15] (see also Sec. III A) are fulfilled. As frequently mentioned above, the theory yields a Gaussian velocity distribution. We have numerically computed, therefore, the velocities (slopes of the levels). The histogram is presented in Fig. 15. Velocities have been compensated for the overall drift so the average velocity vanishes. They also have been rescaled so the variance of the presented distribution is one. One immediately notices a strongly asymmetric shape with a long tail for positive velocities. Clearly, the hydrogen atom in a magnetic field does not obey the theory [15] or its version given in Sec. III.

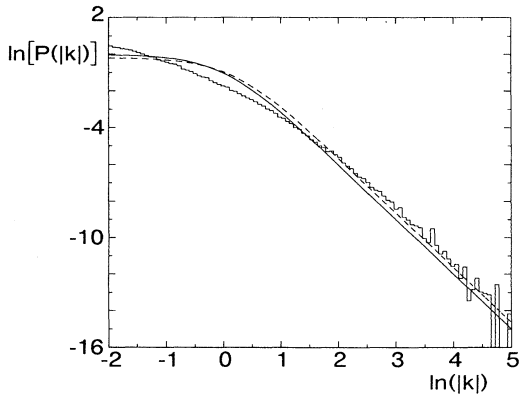

FIG. 14. Same as Fig. 13 but in the logarithmic scale showing the large-k behavior. The solid line represents the *ad hoc* distribution; the dashed line is the rescaled distribution to compensate for the large tail of the velocity distribution. See the discussion in the text and Fig. 15.

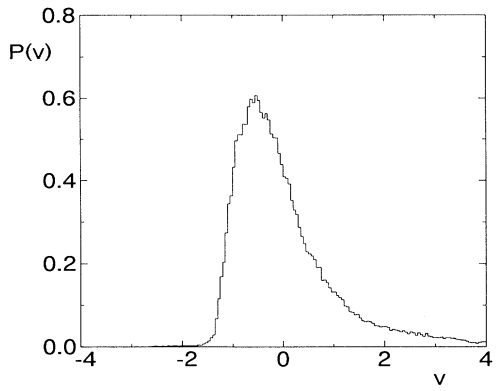

FIG. 15. Normalized velocity distribution for the magnetized hydrogen atom. The horizontal axis scaled to the unit variance. Note the large asymmetry of the curve around the mean $v = 0$ value and the long tail of the distribution.

Let us consider the velocity distribution in more detail. The huge bump around $v = 0$ resembles the Gaussian distribution, provided we neglect the asymmetry due to the tail. In the coordinate frame, in which the overall drift of levels is zero, velocity of a given level changes sign mainly when the level undergoes an avoided crossing. The corresponding curvature should be large. On the other hand, the long tail may be associated with the motion of the scarred states (very abundant in the magnetized hydrogen [6]). Their absolute velocity is typically small (they behave almost linearly with the change of the parameter ε), thus in the moving frame (where average velocity of *all* levels is zero) they acquire a relatively large nonzero component. Thus the tail is related to the "linear regime" of the scarred states motion and, therefore, to the nonuniversal [20] small-curvature regime.

For comparison with the random theory ([15] and Sec. III) this tail may be substracted. Then clearly the variance of velocities becomes smaller. This in turn affects the proper rescaling of the curvatures. Recall that β in the definition of γ_O, Eq. (3.32), is the inverse velocity variance. The effective γ_O should, therefore, be smaller and the dimensionless curvature k, Eq. (3.28), should also be appropriately modified. Instead of shrinking k, we may rescale (expand) the theoretical distribution. The trend obtained by such a procedure is depicted in Fig. 14 by a dashed line. Notice that after the correction of the velocity variance the numerical histogram and theoretical curve practically coincide for large k.

The question remains as to what the origin of the unexpected slope in the stadium-billiard case is, Fig. 12. Further tests in the billiard case would be necessary to draw any definite conclusion. The correspoding velocity distribution should be found. Importantly, strictly speaking, there is no theoretical ground to believe that the tail behavior, as given by Eq. (2.13), should be applicable for strongly scarred systems. Both the theory of [15] and the theory of Sec. III assume the decorrelation of velocities (slopes) and positions (eigenvalues) of the fictitious particles. This is certainly only an approximation for a strongly scarred system. The results for the stadium billiard might be a first indication of the nonuniversality of large-curvature behavior.

D. Nonuniversality of curvature distributions

Let us consider in more detail the small-curvature distribution and its nonuniversality. As discussed above, the accumulation of curvatures around $k = 0$ has been attributed [20] to the strongly scarred "bouncing-ball" eigenstates. Similar effect has been observed for the another "strongly scarred" system, the magnetized hydrogen atom (Fig. 13) supporting this interpretation. The question remains as to whether some simple distribution may, at least partially, simulate the numerically found distributions presented in Figs. 10 and 13.

Fortunately such a distribution is easily at hand. According to Takami and Hasegawa [20] (see also the discussion above), the accumulation of curvatures comes from small curvatures of the "scarred states" in the relatively large intervals of parameter values where these states do not undergo some avoided crossings. The dependence of the energy on the parameter is, in this regime, almost linear. Recall, from the Sec. II, that it is precisely the linear regime which forced us to abandon the linear dependence on the parameter model, Eq. (2.1). Therefore the simple 2×2 model should be applicable to a good approximation for the strongly scarred states, as they are either little affected by other levels or undergo relatively small and narrow avoided crossings.

To construct such a model the theory of [15] cannot be used. What we need now is not a statistical theory in which no limit on λ may be imposed, but rather a standard two-level RMT approach applied to the Hamiltonian, Eq. (2.1). The equation relating the curvature to elements of the Hamiltonian matrix (2.4) for $N = 2$ levels takes the form

$$K_n = \frac{d^2 x_n}{d\lambda^2} = 2\frac{(H_2)_{nm}(H_2)_{mn}}{x_n - x_m}, \qquad n \neq m = 1, 2. \tag{4.10}$$

Let us consider the distribution of $|K|$. The $|x_2 - x_1|$ is equal to the level spacing S. Thus

$$|K| = 2\frac{(H_2)_{21}(H_2)_{12}}{S}. \tag{4.11}$$

Consider the case of small λ, then H_2 in Eq. (2.1) may be considered as a perturbation of H_1. The matrix elements of H_2 are to be calculated in the eigenbasis of $H(\lambda)$. For λ small this basis will be an eigenbasis of H_1 to a good approximation. For almost any H_2 one may therefore assume that the matrix of H_2 will have GOE properties with some variance δ. Its nondiagonal matrix elements will be equal, real, and normally distributed with zero mean. Their product $y = (H_2)_{1,2}(H_2)_{2,1}$, therefore, obeys the Porter-Thomas distribution

$$P_y(y) = \frac{1}{\sqrt{2\pi y\delta}} \exp\left(\frac{-y}{2\delta}\right). \tag{4.12}$$

On the other hand, S is distributed according to the celebrated Wigner form,

$$P_S(S) = \frac{S}{2\sigma^2}\exp\left(-\frac{S^2}{4\sigma^2}\right), \tag{4.13}$$

where σ is the variance corresponding to H_1, in general different from δ. Typically, $\sigma = \pi^{-1/2}$, so the average spacing is equal to one.

The full distribution of curvatures may be obtained in quite a straighforward manner as

$$P_O(|K|) = \int_0^\infty dS \int_0^\infty dy P_S(S) P_y(y) \delta(K - 2y/S), \tag{4.14}$$

which with the help of [30] becomes

$$P_O(|K|) = \frac{3}{(16\sqrt{2\pi}B|K|)^{1/2}} \mathcal{D}_{-5/2}\left(\frac{|K|}{\sqrt{8\pi}B}\right), \tag{4.15}$$

where $B = \sigma/\delta$ and the $\mathcal{D}_p(z)$ function defined by Eq. (3.12). The distribution given by Eq.(4.15) is divergent at $K = 0$ showing that when λ becomes large, the levels behave almost linearly. In this regime, however, the assumption about the smallness of H_2 is not fulfilled. By comparison of Eq. (4.15) with the corresponding expression obtained in the statistical-mechanics model, Eq. (3.16), one notices that the latter is nothing else but the former averaged with the Gaussian of finite width. Clearly, therefore, to remove the singularity at $K = 0$ one may average Eq. (4.15) with the Gaussian weight function, the width of which should be determined by the limits of applicability of the two-level RMT model, i.e., should be related to the mean level spacing.

Even without this averaging we may compare the distribution Eq. (4.15) with numerical data to see whether such a procedure would make sense. One must first determine the free parameter B in Eq. (4.15). This we will do by comparison of its large curvature limit with the limiting distribution given by Eq. (2.13). Such a procedure fixes B value at

$$B = \sqrt{\frac{1}{6\pi\sqrt{2}}}\pi\frac{\bar{\rho}}{\beta}. \tag{4.16}$$

To test how the distribution, Eq. (4.15), fares with respect to the "scarred" low-curvature region we plot it in Fig. 16 together with the stadium-billiard data and the hydrogen atom data. Only the vicinity of small k is shown in Fig. 16 [large-k behavior is fitted, via Eq. (4.16), to the hydrogen data]. One notes that the theoretical curve reproduces quite well the general shape of the data. Of course one should not expect a quantitative agreement, bearing in mind that the theoretical distribution diverges at $k = 0$ and that the data also contain contributions from states not scarred, for which small-curvature behavior is incorrectly described by Eq. (4.15). The result, although being only qualitative, confirms therefore the interpretation of the origin of small-curvature nonuniversality.

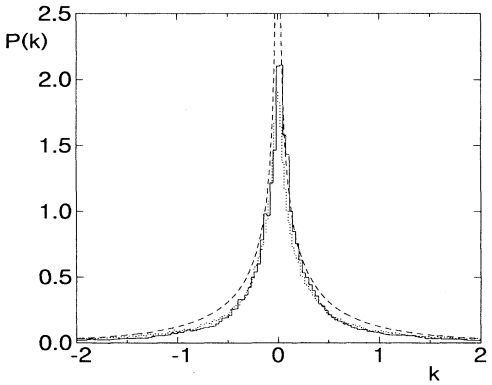

FIG. 16. Comparison of the normalized-curvature distribution for the stadium billiard (solid line) (data courtesy of T. Takami and H. Hasegawa) and the magnetized hydrogen atom (dotted line). Dashed line shows the theoretical distribution, Eq. (4.15) obtained in the two-level RMT. For a discussion see text.

V. SUMMARY

The reader, who has survived with us up to this part, may feel a bit disappointed. We did not present a definite general answer for the statistical behavior of curvatures in classically chaotic systems. On the other hand, several interesting questions have been here, in our opinion, answered and the clear picture of the importance of the curvature distributions to the understanding of the statistical approach to quantally chaotic systems emerges.

The model that enables us to study the curvature distribution (as well as other statistical properties—see, e.g., [13]) in finite-dimensional systems has been developed. The theory is a modification of the statistical-mechanics approach of [15], but for the "contained gas" rather than for the "expanding gas" of the fictitious particles.

Several analytic formulas have been presented which approximate the curvature distributions. Two main approaches have been used: (1) the two-level model realized in the statistical mechanics of the "contained gas," and (2) inspired guess which has led us to simple analytic formulas reproducing very well these parts of the curvature distribution that come from the "random" chaoticlike dynamics.

The failure of 2×2 models to describe, at least approximately, the random part of the curvature distributions is traced to the strong many-level interaction in chaotic systems, or putting it in the language of the fictitious particle dynamics, the long range of the potential coupling the fictitious particles.

The main problem concerning the "random part" of the curvature statistical behavior—the calculation of the appropriate distribution using either the $N = \infty$ model of [15] or the limit of large N in the alternative dynamics of the "contained gas"—remains, however, unsolved. On the other hand, the "inspired guess" formulas Eq. (3.27) fit the data for random dynamics model very well, and the parameters involved in the proposed distributions have the form coming directly from the semicircle law. The proposed expressions should be therefore an

excellent approximation for the random part of the dynamics, if not, by pure chance, an exact result.

We have confirmed the nonuniversal behavior of small curvatures found for a stadium billiard [20] in another prominent system of "quantum chaos" studies, the hydrogen atom in a strong static magnetic field. This results helps us to confirm that the small-curvature accumulation is due to the strong scarring in the system, in agreement with the original interpretation of [20].

From an extreme point of view the nonuniversal behavior of small curvatures may seem to indicate the little significance of the study of their statistical properties. We strongly disagree with such an opinion. Rather one should think of using the additional information contained in the curvature distribution to get a quantitative information about the system studied. Otherwise the curvature distribution would yield just the same information as it is already contained in, e.g., level-spacing distributions.

We suggest that the curvature distribution may be used to measure quantitatively how strongly a given physical system is scarred. The related problem of measuring the content of a scar in an individual wave function [34] or a group of states [35] has been addressed recently. How to define properly such a measure remains, at present, an open question which we shall study in the future.

The present results allow for only a qualitative classification of the different systems with respect to scarring. The results indicate that the excess at $k \approx 0$ of the numerical histogram over the value given by the *ad hoc* expressions, Eq. (3.27) may be used to roughly estimate the strength of scarring. It is known [36] that there is some, not too strong, scarring in the kicked-top model. This is in agreement with Fig. 4, which shows that the low curvature excess above the guessed distribution is quite small. In this aspect, the second time-dependent Hamiltonian system considered, the kicked rotator (Fig. 13), shows a larger "nonuniversal" contribution, which suggests that, for the used values of the appropriate parameters, stronger scarring appears in this system. By comparison, autonomous systems, such as the magnetized hydrogen atom and, in an even higher degree, the stadium billiard, show much stronger scarring (Fig. 16).

Interestingly, for systems belonging to the unitary symmetry class (both kicked top, Fig. 5, and kicked rotator, Fig. 12) no excess above the random motion predictions appears. The only nonrandom data for the symplectic universality class show (Fig. 6) again some excess above the *ad hoc* distribution limit. Experimentally, i.e., numerically, as far as we know, scarring has been observed only for the systems belonging to the orthogonal universality class.

As seen from the above, statistical analysis of the curvature distributions is not only important due to its possible direct significance for measurable quantities as, e.g., in solid states application (see Introduction), but it provides very important information about the dynamics of the system studied. To use the information contained in the curvature distribution more data for other model and realistic systems would be most welcome.

ACKNOWLEDGMENTS

This paper would not take its present form without the outstanding help of Professor Hiroshi Hasegawa, Professor Fritz Haake, Mr. Toshiya Takami, and Mr. Dirk Saher who supplied us, on request, with their published data on the kicked-top model [16], the kicked-rotator, and the stadium billiard systems [20]. We deeply thank them for their cooperation and the continuing interest in this work. We are grateful to Professor Oriel Bohigas and Dr. Marek Kuś for interesting discussions. J.Z. thanks his colleagues at the Laboratoire de Spectroscopie Hertzienne for hospitality and the Ministère de la Recherche et de la Technologie for the financial support. Support of the Polish Committee of Scientific Research under Grant No. 200799101 (J.Z.) is acknowledged. Laboratoire de Spectroscopie Hertzienne de l'Ecole Normale Supérieure et de l'Université Pierre et Marie Curie is "Unité Associée 18 du Centre National de la Recherche Scientifique."

* Permanent address: Instytut Fizyki, Uniwersytet Jagielloński, ulica Reymonta 4, 30-059 Kraków, Poland.

[1] C. E. Porter, *Statistical Theories of Spectra. Fluctuations* (Academic, New York, 1965).
[2] M. L. Mehta, *Random Matrices* (Academic, New York, 1991).
[3] O. Bohigas and M. J. Giannoni, in *Chaotic Motion and Random Matrix Theories*, edited by J. S. Dehesa, J. M. G. Gomez, and A. Polls, Lecture Notes in Physics Vol. 209 (Springer, Berlin, 1984), p. 1.
[4] F. Haake, *Quantum Signatures of Chaos* (Springer, Berlin, 1991).
[5] O. Bohigas in *Chaos and Quantum Physics*, 1899 Les Houches Lecture Session LII, edited by M.-J. Giannoni, A. Voros, and J. Zinn-Justin (North-Holland, Amsterdam, 1991), p.87.
[6] For a review see, e.g., D. Delande, in *Chaos and Quantum Physics* (Ref. [5]), p. 665.
[7] I. C. Percival, J. Phys. B **6**, L229 (1973).
[8] N. Pomphrey, J. Phys. B **7**, 1909 (1974).
[9] D. W. Noid, M. L. Koszykowski, M. Tabor, and R. A. Marcus, J. Chem. Phys. **72**, 6169 (1980).
[10] M. Wilkinson, J. Phys. A **22**, 2795 (1989).
[11] J. Goldberg and W. Schweizer, J. Phys. A **24**, 2785 (1991).
[12] J. Zakrzewski and M. Kuś, Phys. Rev. Lett. **67**, 2749 (1991).
[13] J. Zakrzewski, D. Delande, and M. Kuś, following paper, Phys. Rev. E **47**, xxxx (1993).
[14] P. Gaspard, S. A. Rice, and K. Nakamura, Phys. Rev. Lett. **63**, 930 (1989).
[15] P. Gaspard, S. A. Rice, H. J. Mikeska, and K. Nakamura, Phys. Rev. A **42**, 4015 (1990).
[16] D. Saher, F. Haake, and P. Gaspard, Phys. Rev. A **44**, 7841 (1991).
[17] M. Kuś, R. Scharf, and F. Haake, Z. Phys. B **66**, 129

(1987).
[18] F. Haake, M. Kuś, and R. Scharf, Z. Phys. B **65**, 381 (1987).
[19] R. Scharf, B. Dietz, M. Kuś, F. Haake, and M. V. Berry, Europhys. Lett. **5**, 383 (1988).
[20] T. Takami and H. Hasegawa, Phys. Rev. Lett. **68**, 419 (1992).
[21] K. Nakamura and M. Lakshmanan, Phys. Rev. Lett. **61**, 247 (1988).
[22] G. Lenz and F. Haake, Phys. Rev. Lett. **65**, 2325 (1990).
[23] G. Lenz and F. Haake, Phys. Rev. Lett. **67**, 1 (1991).
[24] E. Heller, Phys. Rev. Lett. **53**, 1515 (1984).
[25] P. Pechukas, Phys. Rev. Lett. **51**, 943 (1983).
[26] T. Yukawa, Phys. Rev. Lett. **54**, 1883 (1985); Phys. Lett. A **116**, 227 (1986).
[27] K. Nakamura and M. Lakshmanan, Phys. Rev. Lett. **57**, 1661 (1986).
[28] J. Gibbons, T. Hermsen, and S. Wojciechowski, Phys. Lett. **94A**, 251 (1983); S. Wojciechowski, *ibid.* **111A**, 101 (1985); Phys. Scr. **34**, 304 (1986).
[29] Using the analogy with the fictitious particle dynamics one should rather speak of "accelerations" of particles instead of curvatures of levels. In the following we use the latter as having a more direct physical meaning.
[30] I. S. Gradshteyn and I. M. Ryzhik, *Table of Integrals, Series and Products* (Academic, New York, 1980).
[31] Strictly speaking, it is common to call the system of fictitious particles interacting according to (2.9) or (3.3) a gas. More correctly one should speak of a quasicrystalline phase [5], see also X. Yang and J. Burgdörfer (unpublished). Neverthless, we shall use in the following the traditional notion of "gas" [25] for the convenience of the reader.
[32] Takami and Hasegawa use $K\bar{\rho}/\beta$ as in [15], thus our dimensionless curvature k Eq. (3.28) differs by a factor π for the orthogonal and 2π for the unitary rotator.
[33] H. Friedrich and D. Wintgen, Phys. Rep. **183**, 37 (1989).
[34] D. Wintgen and A. Honig, Phys. Rev. Lett. **63**, 1467 (1989).
[35] D. Delande and J.C. Gay, Phys. Rev. Lett. **59**, 1809 (1987).
[36] M. Kuś, J. Zakrzewski, and K.Życzkowski, Phys. Rev. A **43**, 4244 (1991).